Arabian Journal of Chemistry (2020) 13, 4404–4416

King Saud University

Arabian Journal of Chemistry

www.ksu.edu.sa
www.sciencedirect.com

ORIGINAL ARTICLE

SPR effect of Au nanoparticles on the visible photocatalytic RhB degradation and NO oxidation over TiO_2 hollow nanoboxes

Lianqing Chen [a,b], Lijun Tian [a], Xuan Zhao [a], Zhao Hu [a], Jiajie Fan [c], Kangle Lv [a,*]

[a] *Key Laboratory of Catalysis and Energy Materials Chemistry of Ministry of Education & Hubei Key Laboratory of Catalysis and Materials Science, South-Central University for Nationalities, Wuhan 430074, China*
[b] *Department of Chemistry, University of Wisconsin-Platteville, Platteville 53818, United States*
[c] *School of Materials Science and Engineering, Zhengzhou University, Zhengzhou 450001, China*

Received 23 April 2019; accepted 12 August 2019
Available online 10 September 2019

KEYWORDS

Au;
TiO_2;
Hollow nanobox;
Surface plasmon resonance;
Photocatalysis

Abstract Three-dimensional (3D) TiO_2 hollow structures have attracted much attention due to their unique properties. However, the large bandgap of (3.2 eV) results in the fact that anatase TiO_2 photocatalyst can only be excited by UV light, which only accounts for 3–5% of the solar energy. On considering that nobel metallatic nanomaterials can harvest visible light due to surface plasmon resonance (SPR) effect, in this paper, three kinds of Au nanoparticles with different morphologies, namely Au nanospheres (Au-NSs), Au nanorods (Au-NRs) and Au nanopentogons (Au-NPs) were prepared and used as photosensitizers to modified TiO_2 hollow nanoboxes (TiO_2-HNBs), aiming to explore high efficient visible-light-responsive photocatalyst. The photoreacitivty of Au/TiO_2-HNBs was evaluated by photoctalytic oxidation of Rhodamine B (RhB) and NO under visible irradiation ($\lambda > 420$ nm). It was found that the visible photoreactivity of TiO_2-HNBs was greatly enhanced after modified with Au nanoparticles, and TiO_2-HNBs loaded with Au-NRs exhibit the highest visible photocatalytic activity towards both RhB degradation and NO oxidation. Upon visible irradiation, SPR effect induces the production of hot electrons from the Au nanoparticles, which can further transfer to the conduction band of TiO_2-HNBs to produce superoxide radicals ($\cdot O_2^-$), resulting in an efficient separation of photo-generated electron-hole

* Corresponding authors at: Key Laboratory of Catalysis and Energy Materials Chemistry of Ministry of Education & Hubei Key Laboratory of Catalysis and Materials Science, South-Central University for Nationalities, Wuhan 430074, China.
E-mail addresses: lqchen@mail.scuec.edu.cn (L. Chen), lvkangle@mail.scuec.edu.cn (K. Lv).
Peer review under responsibility of King Saud University.

Production and hosting by Elsevier

https://doi.org/10.1016/j.arabjc.2019.08.011

pairs. The photoreactivity of Au-NRs/TiO_2-HNBs towards RhB degradation almost keeps unchanged even after recycling used for 5 times, indicating that it is promising to be use in practical applications.

1. Introduction

Semiconductor photocatalysis has attracted much attention since the report of water-splitting to produce hydrogen over illuminated-TiO_2 by Fujishima in 1972 (Fujishima and Honda, 1972; Yang et al., 2017b; Low et al., 2017; Li et al., 2018a; Di et al., 2018). Among all the photocatalytic materials, TiO_2 is considered to be the most promising semiconductor photocatalyst due to its unique optical and electronic properties, relatively high catalytic activity, non-toxicity, chemical stability and low costs (Qi et al., 2017; Negrín-Montecelo et al., 2018; Zou et al., 2017; Priebe et al., 2017; Rahul and Sandhyarani, 2017). Upon irradiation, photo-generated electrons and holes will migrate from the bulk to the surface of the excited TiO_2. The holes can directly oxidize the adsorbed organics, or surface adsorbed water to produce high reactive hydroxyl radicals (·OH), while electrons can be captured by dissolved oxygen to produce super oxygen radicals). Both ·OH and $\cdot O_2^-$ are reactive oxygen species (ROSs) that can attack organic pollutants, resulting in their degradation and minerization (Schneider et al., 2014). However, the large band-gap (3.2 eV for anatase TiO_2) and low quantum efficiency hampers the pratical applications of TiO_2 photocatalysis (Sheng et al., 2014; Duan et al., 2018; Low et al., 2018b). To extend the light-responsive range and/or improve the photocatalytic activity of TiO_2, many strategies have been used such as doping TiO_2 with metal (Yang et al., 2017c) or nonmetal ions (Zhang et al., 2018a; Li et al., 2018b), coupling TiO_2 with other semiconductor to form heterojunctions (Li et al., 2017a; Huang et al., 2015; Meng et al., 2017), surface modification of TiO_2 with fluoride ions (Luan et al., 2013; Lv et al., 2012b) or carbon materials (Lv et al., 2017; Wang et al., 2014; Low et al., 2018c). In 2008, Lu et al. reported the fabrication anatase TiO_2 crystals with exposed high photoreactive {0 0 1} facets using HF as morphology-controlling agent, which is an important breakthrough in preparation of high efficient TiO_2 photocatalyst (Yang et al., 2008; Wang et al., 2018; Akple et al., 2015).

In the last several decades, much work has been devoted to fabricate hollow structured TiO_2 due to its low density, high photoreactivity and excellent permibility (Lv et al., 2012b; Lou et al., 2008; Ning et al., 2018; Zhang et al., 2017; Low et al., 2018a; Yang et al., 2017a). Hollow structured TiO_2 photocatalysts have been prepared by hard templated (Lan et al., 2015; Li et al., 2009) and template-free methods (Lei et al., 2015; Dwivedi and Dutta, 2012). We have reported the fabrication of high photoreactive TiO_2 hollow nanoboxes (TiO_2-HNBs) assembly from TiO_2 nanosheets with exposed high energy {0 0 1} facets by solvothermal treatment of cubic $TiOF_2$ using alcohol as solvent (Huang et al., 2013). However, TiO_2-HNBs still can only be excited by UV light, which only accounts for 3–5% of the solar energy. Exploration of high efficient visible-light-responsive TiO_2-HNBs to make full use of solar light is of great importance (Zhao et al., 2018; Zhang et al., 2018b).

Recently, surface plasmon resonance (SPR) effect of metals such as Au, Ag, Pd and Bi under the visible light irradiation has been used for photocatalysis (Wanbayor and Ruangpornvisuti, 2012; Wu et al., 2009; Ma and Li, 2018; He et al., 2018; Damato, 2018; Zhang et al., 2019). For example, it was reported the observation of huge local electric field enhancement at the surface of Au nanoparticles due to the strong interaction of the electric and magnetic field of light on Au nanoparticles (Wanbayor and Ruangpornvisuti, 2012). Under visible irradiation, the plasmon-induced hot electrons can injected into the conduction band of the contacted semiconductors such as TiO_2, therefore improving the photoreactivity. SPR effect typically depends on chemical composition, size and shape of the metal nanoparticles in contact with TiO_2. On considering that SPR effect of Au nanoparticles can be used to sensitize TiO_2-HNBs, in this paper, visible-light-responsive Au nanoparticles modified TiO_2-HNBs hybridized photocatalyst (Au/TiO_2-HNBs) were prepared. Although SPR effect of Au nanoparticles has been used to extend the visible-light responsive range of TiO_2 photocatalyst, many studies focused on the study of Au particle sizes (Yu et al., 2006; Golabiewska et al., 2016), composition (Verbruggen et al., 2014) or the calcination temperature (Acik et al., 2014). Here we studied the effect of the Au morphology, namely Au nanorods (Au-NRs), Au nanospheres (Au-NSs) and Au nanopentagon (Au-NPs), on the visible photocatalytic activity of Au/TiO_2-HNBs.

2. Experimental

2.1. Preparation of TiO_2-HNBs

We prepared $TiOF_2$ precursor according to the our previous report (details see S1 in Supporting Information) (Huang et al., 2013). TiO_2-HNBs was synthesized by solvothermal treatment of the prepared $TiOF_2$. Specifically, 1.0 g of $TiOF_2$ powders were homogeneously dispersed in 40 ml of anhydrous ethanol by ultrasonicating for 10 min, which was then transferred into a 50 ml Teflon-lined autoclave and heated at 200 °C for 12 h. The produced white powders were washed and dried in an oven at 60 °C for 6 h.

2.2. Preparation of Au nanoparticles

We prepared three kinds of Au nanoparticles, namely Au nanospheres (Au-NSs), Au nanorods (Au-NRs) and Au-nanopentagons (Au-NPs) (Golabiewska et al., 2016). There are two steps for the synthesis of each Au nanoparticles. The first step is the preparation of Au seed solution, and the second

step is the growth of Au nanoparticles. The details for the preparation of Au seed solution can be found from Part S2 of the Supporting Information.

For preparation of Au nanospheres (Au-NSs), 550 μL of ascorbic acid (0.1 mol L^{-1}) and 100 μL of Au-NSs seed solution were added into a flask containing 100 ml of $HAuCl_4$ (0.5 mmol L^{-1}) and 150 ml of hexadecyl trimethyl ammonium bromide (0.2 mol L^{-1}) under magnetic stir. The resulted burgundy solution was kept still 30 °C for 24 h, and followed by centrifugation to remove supernant.

For preparation of Au nanorods (Au-NRs), 5 ml of $HAuCl_4$ (0.5 mmol L^{-1}), 70 μL of L-ascorbic acid (78.8 mmol L^{-1}) and 12 μL of Au-NRs seed solution were added into a flask containing 5 ml of hexadecyl trimethyl ammonium bromide (0.2 mol L^{-1}) and 100 ml of $AgNO_3$ (0.40 mmol L^{-1}) under magnetic stir. The resulted solution was kept still at 28 °C for 30 h, and followed by centrifugation to remove supernant.

For preparation of Au nanopentagons (Au-NPs), 550 μL of ascorbic acid, 550 μL NaOH (0.2 mol L^{-1}), 0.75 ml NaI (0.2 mol L^{-1}), and 100 μL of Au-NPs seed solution were added into a flask containing 100 ml of $HAuCl_4$ (0.5 mmol L^{-1}) and 50 ml of hexadecyl trimethyl ammonium bromide (0.2 mol L^{-1}) under magnetic stir. The resulted orange solution was kept still at 30 °C for 24 h, which is followed by centrifugation to remove supernant.

2.3. Deposition of Au nanoparticles on TiO_2-HNBs

100 μL of $NH_3{\cdot}H_2O$ (28 wt%) and 50 μL of 3-mercaptopropionic acid (MPA) were added into 50 ml of water under magnetic stir. Then, 0.1 g of TiO_2-HNBs powders and the prepared Au-NRs (Au-NSs or Au-NPs) were added into the mixed solution. 30 min later, the suspensions were kept still for 12 h. The resulted solution was centrifuged to remove supernant and washed with water. The precipitates were dried at 60 °C for 12 h, followed by calcination at 200 °C for 2 h. The prepared sample is denoted as Au-NRs/TiO_2-HNBs (Au-NSs/TiO_2-HNBs or Au-NPs/TiO_2-HNBs).

2.4. Characterization

Transmission electron nanoscopy (TEM) and scanning electron nanoscopy (SEM) images were obtained to observe the morphology of the samples. The former was performed on a JSM-6700F field emission SEM (Hitachi, Japan) at an accelerating voltage of 10 kV, while the latter was taken on a transmission electron nanoscope (Tecnai G^2 20, USA) at 200 kV. Powder X-Ray diffraction (XRD) patterns were obtained on an X-ray diffractometry (D8-advance, Bruker; Germany) to determine the crystal phase of the prepared samples. UV-Vis diffuse reflectance spectra (DRS) of the samples were obtained on UV-Vis spectrophotometer (UV2600, Shimadzu, Japan) using $BaSO_4$ as the reflectance standard. Fourier Transform infrared spectroscopy (FTIR) spectrum of the photocatalyst was measured through Nexus 470 FT-IR (Shimadzu, Japan). The surface area and pore structure of the photocatalyst was measured in a nitrogen-adsorption instrument (ASAP 2020, USA). X-ray photoelectron spectra (XPS) were performed on a Multilab 2000 XPS system with a monochromatic Mg K*a* source.

2.5. Evaluation of the photocatalytic activity

The photocatalytic activity of the photocatalyst was evaluated by decomposition of organic dye Rhodamine (RhB) and NO oxidation.

For RhB degradation, cyclindrical Pyrex flask was used as the photoreactor. 50 mg of the photocatalyst was dispersed in 50 ml of RhB solution (1.0×10^{-5} mol L^{-1}). After being ultrasonicated and stirred in the dark for overnight to establish the adsorption-desorption equilibrium, the suspensions were illuminated by an Xe lamp (300 W) with a cut-off filter ($\lambda > 420$ nm). At the given time intervals, 3.0 ml of suspension sample was taken and centrifuged to remove the photocatalyst particles. The concentration of RhB in filtrate was monitored by UV–Vis spectroscopy at 554 nm.

Photocatalytic oxidation of NO was performed in a flow reactor at ambient temperature (Zhao et al., 2018; Li et al., 2017b; Li et al., 2018c; Li et al., 2018d). The volume of the rectangular reactor is 4.5 L. An visible LED lamp emitted mainly at 480 nm is used as the light source. Firstly, 0.1 g of the photocatalyst was dispersed in 30 ml of deionized water under sonication, which was then transferred to a culture dish with a diameter of 9.0 cm. The dish with sample was then heated at 60 °C for 3 h to thoroughly evaporate water. After cooled down to room temperature, the dish was moved into the reactor. NO gas was supplied from a compressed gas cylinder having 50 ppm of NO (N_2 balance), and air stream produced from a zero-air generator was used for diluting the initial NO concentration to about 600 ppb. In a gas blender, the gas streams were totally premixed, the gas flow rate was setting as 1.0 L·min^{-1} by employing a mass flow controller. When the gas system can reach adsorption-desorption balance, turning on the lamp. The concentrations of NO from the outlet of the reactor was online monitorred by a chemiluminescence NO_x analyzer (Advanced Pollution Instrumentation, Teledyne Technol., Model T 200).

3. Results and discussion

3.1. Morphologies of the photocatalysts

Scheme 1 shows the process for the fabrication of Au nanoparticles modified TiO_2-HNBs. The first step (step a) is the preparation of cubic $TiOF_2$ nanocrystals according to our previous report (Huang et al., 2013). The second step (step b) is modified TiO_2-HNBs with 3-mercaptopropionic acid (MPA). As MPA contains both carboxyl group (—COOH) and thiol group (—SH). Carboxyl group and thiol group can complex with TiO_2 and Au nanoparticles, respectively. Therefore, using MPA as a media, Au nanoparticles can strongly anchor on the surface of TiO_2-HNBs. The third step (step c) is adsorption of Au nanoparticles from solution to the surface of TiO_2 *via* MPA. The forth step (step d) is removal of MPA by calcination. By using this strategy, Au nanoparticles can deposit on the surface of TiO_2-HNBs.

Fig. 1 shows the SEM and TEM images of the prepared $TiOF_2$ precursor. It can be seen that these $TiOF_2$ precursor has cubic morphology, and the side lengths of $TiOF_2$ cubes are about 200–300 nm. After heat treatment of these $TiOF_2$ precursor in anhydrous ethanol at 200 °C for 12 h, $TiOF_2$ transforms into hollow structured TiO_2 (TiO_2-HNBs) by a

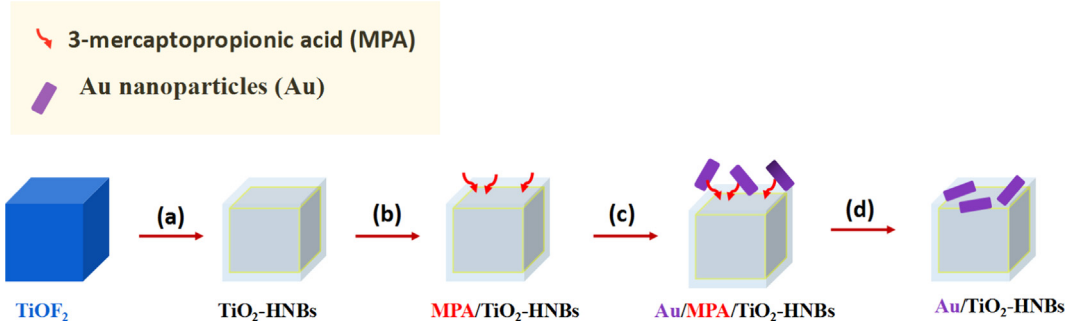

Scheme 1 Strategy for the fabrication of Au nanoparticles modified TiO_2-HNBs: (a) calcination, (b) surface modification of TiO_2-HNBs with MPA, (c) capture of Au nanoparticles via MPA, and (d) removal of MPA by calcination.

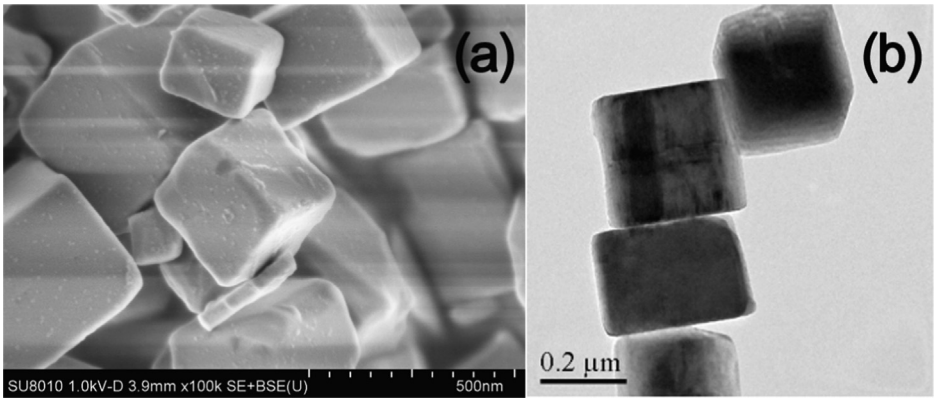

Fig. 1 SEM (a) and TEM (b) images of $TiOF_2$.

self-templated in situ transformation process, where water comes from the dehydration of alcohol (eq. (1)) (Huang et al., 2013).

$$2C_2H_5OH \rightarrow C_2H_5OC_2H_5 + H_2O \quad (1)$$

$$TiOF_2 + H_2O \rightarrow TiO_2 + 2HF \quad (2)$$

The hollow structures of the formed TiO_2 can be clearly seen from Fig. 2. The formed TiO_2-HNBs hydrolyzed from $TiOF_2$ cubes are infact assembled from anatase TiO_2 nanosheets with exposed {0 0 1} facets as HF can act as shape-directing reagent for high energy faceted TiO_2 (Wang et al., 2010; Liang et al., 2017; Shi et al., 2018).

Fig. 3 compares the morphology of the Au nanoparticles, from which Au nanorods (Fig. 3a and b), Au nanospheres (Fig. 3c and d) and Au nanopentagons (Fig. 3e and f) can be clearly observed. Therefore, Au nanoparticles with different morphologies were successfully synthesized.

Fig. 4 shows the TEM and SEM images of the prepared TiO_2-HNBs after loaded with Au-NRs (a and b), Au-NSs (c and d) and Au-NPs (e and f). It can be seen that all these Au nanoparticles strongly anchor on the surface of TiO_2-HNBs. From the elemental maps of Au-NRs/TiO_2-HNBs sample, we can clearly see the homogeneous dispersion of Ti, O and Au elements (Fig. 5), further confirms the successful deposition of Au over TiO_2-HNBs.

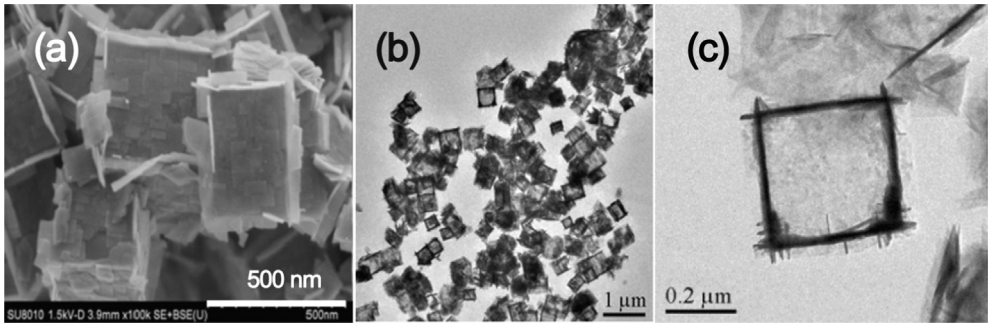

Fig. 2 SEM (a) and TEM (b and c) of TiO_2-HNBs.

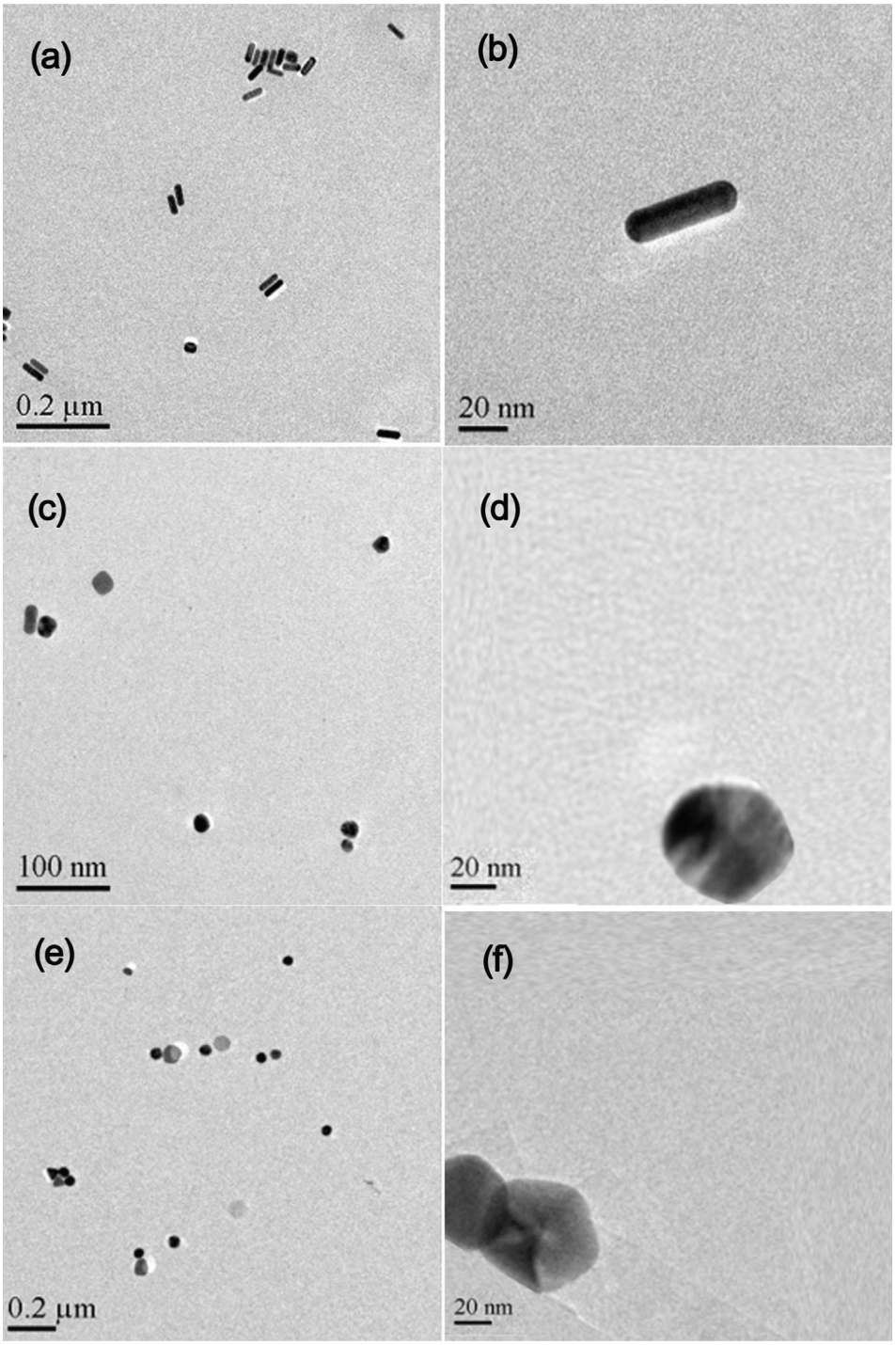

Fig. 3 TEM images of Au nanopartiles with different mophologies: nanorods (a and b), nanospheres (c and d) and nanopentogons (e and f).

3.2. Phase structure and UV-visible absorption spectrum

Fig. 6 exhibits the phase structures of prepared TiO_2-HNBs before and after loaded with Au nanoparticles. It can be seen that there is a strong diffraction peak at $2\theta = 25.3°$ for all the photocatalysts, indicating the production of anatase TiO_2. The diffraction peaks for metal Au are not obvious for all the Au/TiO_2-HNBs hybridized photocatalysts, possibly due to the small particle sizes of Au nanoparticles.

Light harvesting ability is of great importance to the photocatalytic activity of the photocatalyst. Therefore, the UV-visible absorption spectra of the samples are compared, and the results are shown in Fig. 7. Although all samples have similar absorption in UV region, the the absorption in visible

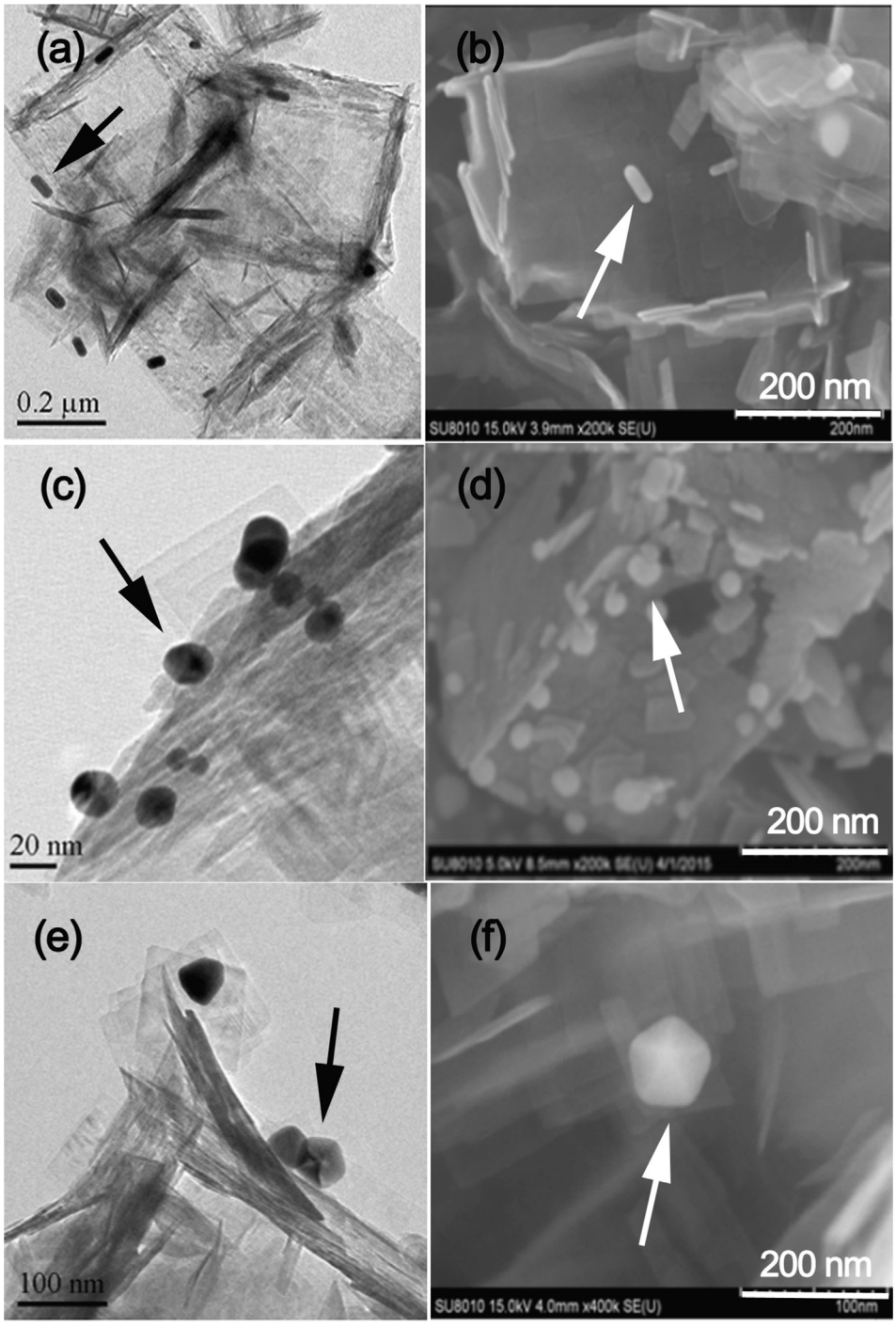

Fig. 4 TEM and SEM images for Au-NRs/TiO_2-HNBs (a and b), Au-NSs/TiO_2-HNBs (c and d) and Au-NPs/TiO_2-HNBs (e and f), and arrows indicating the presence of Au nanoparticles.

region is greatly improved after loading with Au. The enhanced absorption of Au/TiO_2-HNBs can be ascribed to the SPR effect of Au nanoparticles, originating from the interaction of the electric and magnetic field of light on Au nanoparticles (Wu et al., 2009). This SPR effect of Au nanoparticles can be used to sensitize TiO_2-HNBs, enhancing the visible photoreactivity of TiO_2-HNBs. From Fig. 7, we can also see that Au-NRs/TiO_2 exhibits the largest absorption in visible region with two absorption peaks centering at 528 nm and 755 nm, reflecting the strongest SPR effect of Au-NRs. SPR spectra of noble metallic particles can be tuned from near-UV to visible and even mid-infrared region by tailoring their sizes and shapes (Yuan et al., 2007; Borisyuk et al., 2012). As for Au, the particle morphology plays a more significant role on the properties of the SPR band than size. According to the study of Yuan et al., Au particles with sharp apexes such as thorny Au nanoparticles exhibit obvious red-shift of the SPR peak when compared with Au spherical

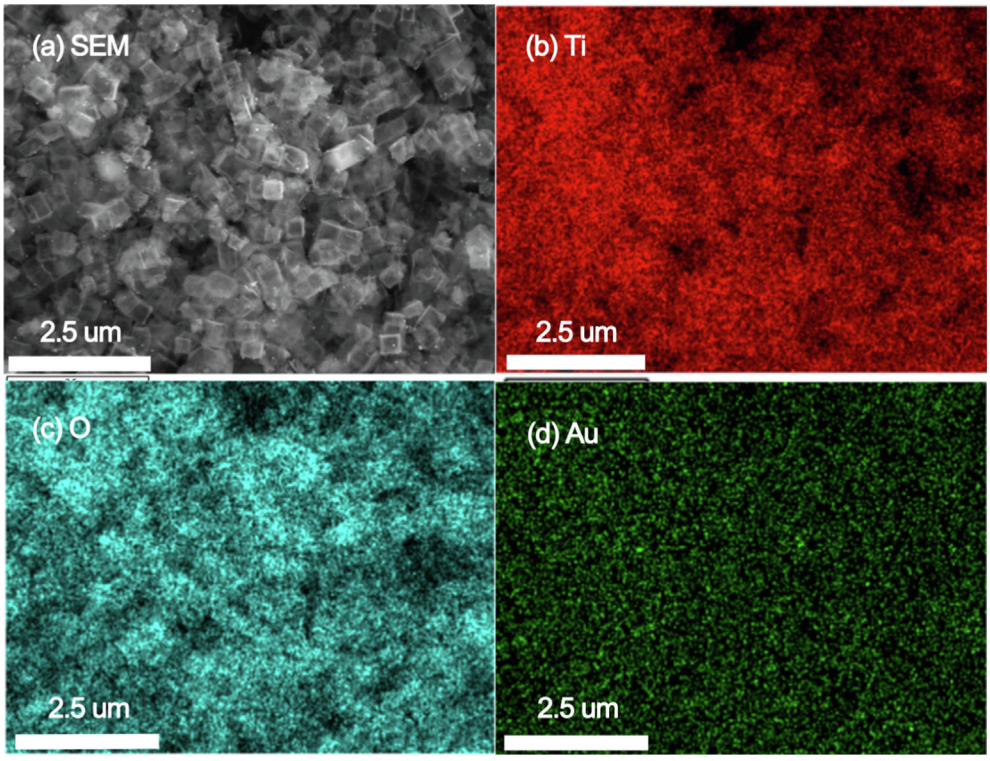

Fig. 5 Elemental maps of Au-NRs/TiO_2-HNBs.

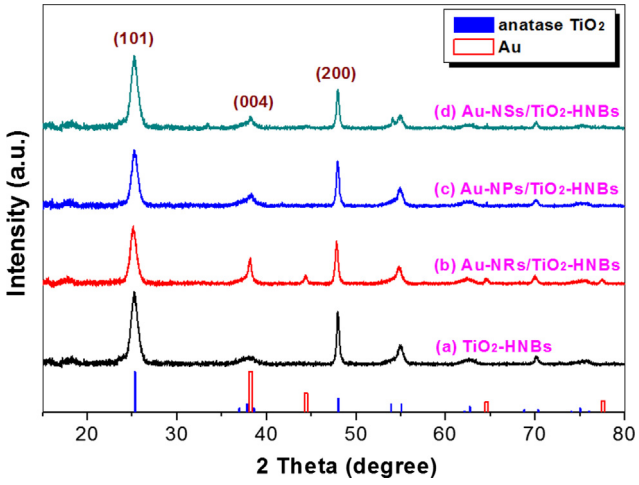

Fig. 6 XRD patterns of the photocatalysts, together with the expected peaks for Au (JCPDF No. 65-2870) and anatase TiO_2 (JCPDF No. 621-1272).

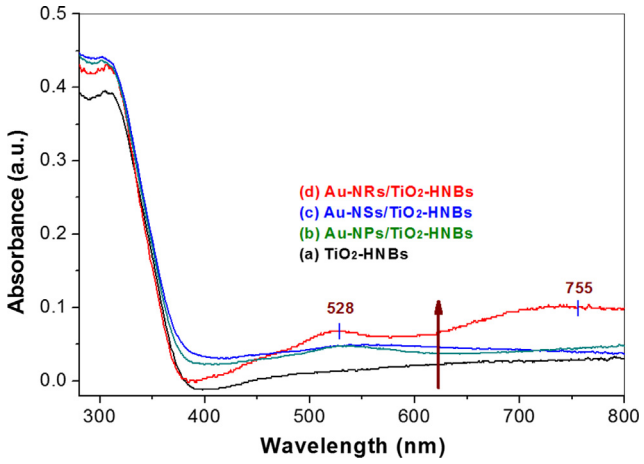

Fig. 7 UV–visible diffuse reflectance spectra of the photocatalysts.

particles (Yuan et al., 2007). Because Au-NRs have the largest aspect ratio, it is not hard to understand that Au-NRs/TiO_2-HNBs exhibit the largest visible absorption due to the strongest SPR effect of Au-NRs when compared with that of Au-NPs and Au-NSs (Figs. 4 and 7).

3.3. FTIR and XPS analysis

Fig. 8 shows the infrared absorption spectra of the photocatalysts. It can be seen that all samples have similar FTIR absorption spectra. The strong absorption peak at about 500 cm^{-1} originates from the stretching vibration of Ti-O bond (Zhao et al., 2018). The absorption peak at 1636 cm^{-1} is attributed to the vibration of Ti—O—Ti bond, while the absorption peak centering at 3438 cm^{-1} is the typical vibration of O—H. Note that there is no obvious characteristic peaks in the range of 2600–2500 cm^{-1} and 1680–1720 cm^{-1}, corresponding to the vibrations for S—H and C═O group (Panayotov et al., 2011), respectively. This indicates that MPA was totally removed from the surface of TiO_2-HNBs.

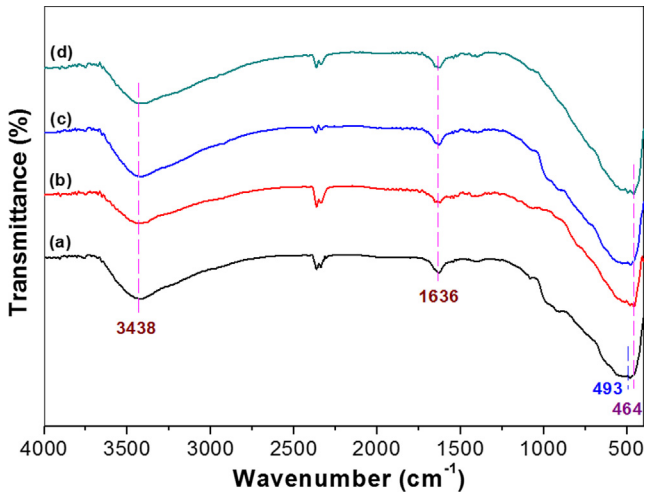

Fig. 8 FTIR spectra of the photocatalysts for pristine TiO_2-HNBs (a), Au-NRs/TiO_2-HNBs (b), Au-NSs/TiO_2-HNBs(c) and Au-NPs/TiO_2-HNBs(d).

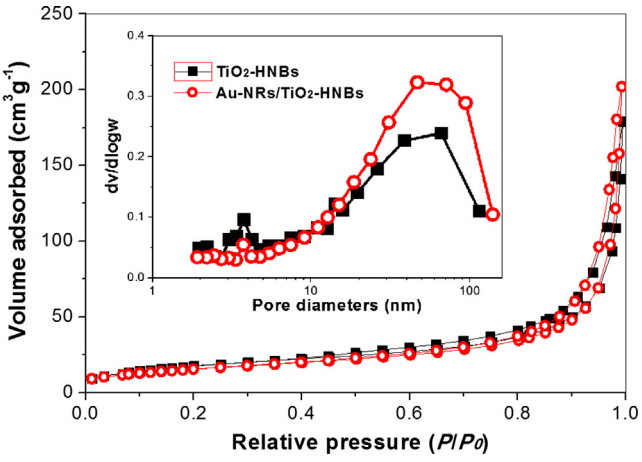

Fig. 10 Nitrogen sorption isotherms and corresponding pore size distribution curves (inset) for TiO_2-HNBs before and after loaded with Au-NRs.

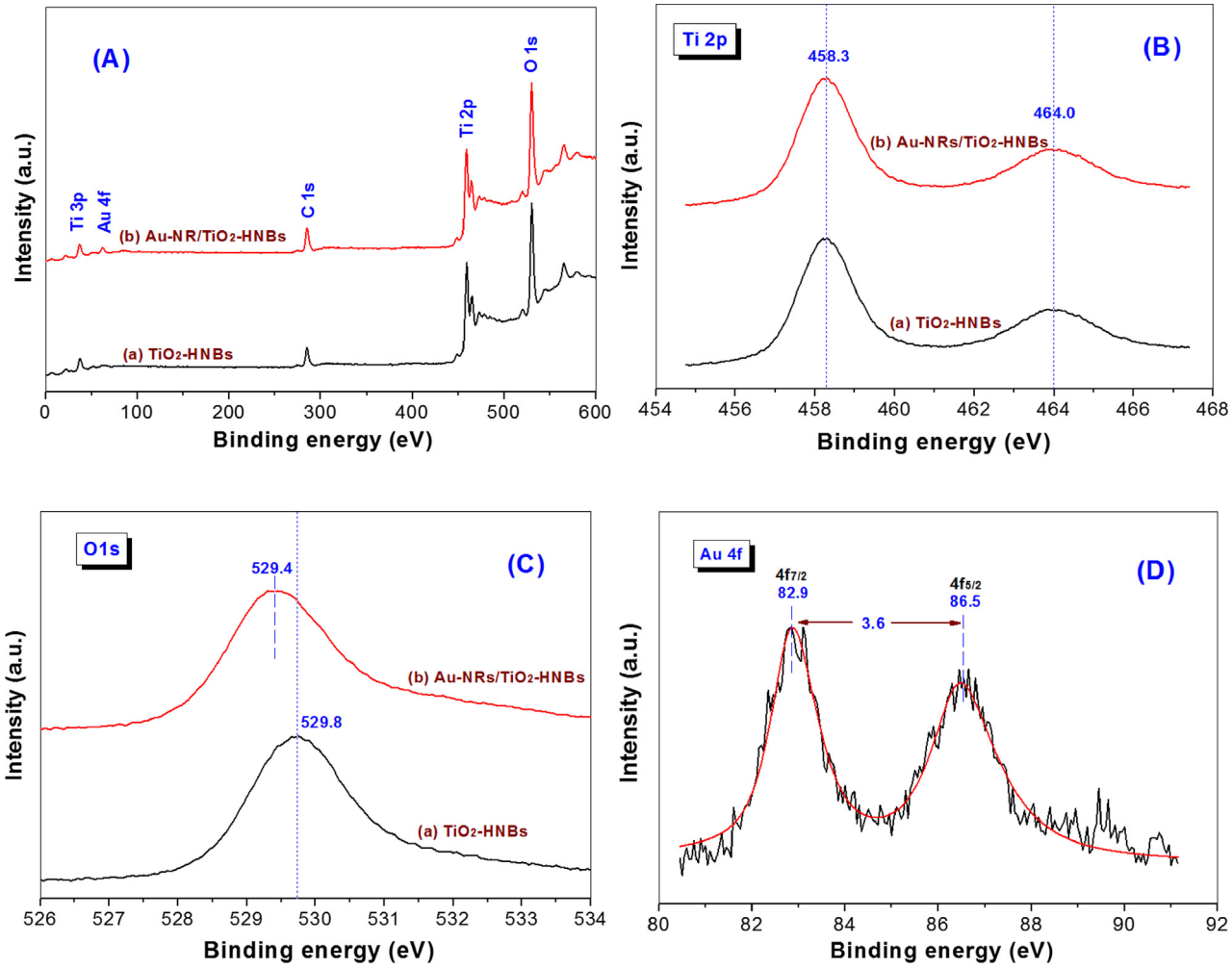

Fig. 9 XPS survey spectra (A) and corresponding high resolution XPS spectra in Ti 2p (B), O 1s (C) and Au 4f (D) regions for pristine TiO_2-HNBs and Au-NRs/TiO_2-HNBs.

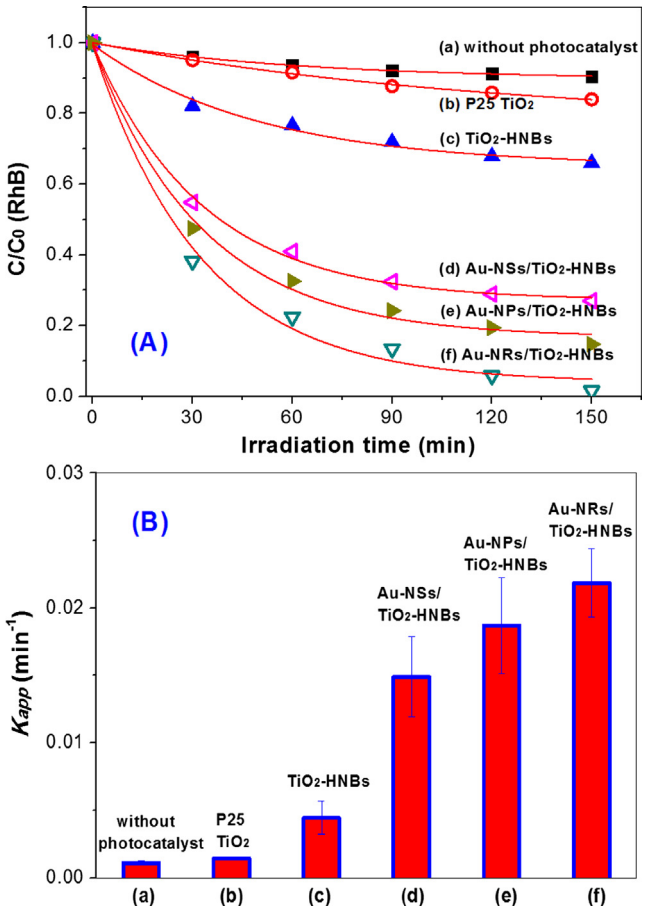

Fig. 11 Visible photocatalytic degradation curves of RhB over different photocatalysts (A) and comparison of the corrsponding rate constants (B).

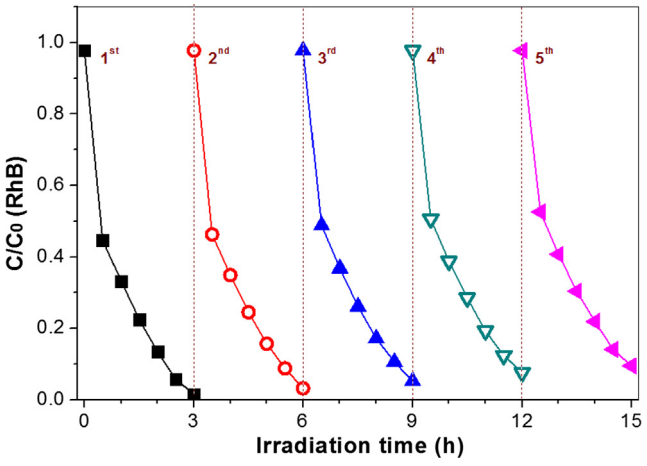

Fig. 12 Visible photocatalytic degradation curves of RhB by repeating use of Au-NRs/TiO_2-HNBs as photocatalyst.

Fig. 9A compares the XPS spectra between TiO_2-HNBs and Au-NRs/TiO_2-HNBs. It can be seen that both samples contain Ti, O and small amount of C elements with binding energies of 458 eV (Ti 2p), 530 (O 1s) and 285 eV (C 1s), respectively. A small peak with binding energy of 83 eV, corresponding to Au 4f (Yuan et al., 2007), was also observed from Au-NRs/TiO_2-HNBs, indicating that Au was successfully deposited on the surface of TiO_2-HNBs.

The high resolution XPS spectra in Ti 2p and O 1s regions are shown in Fig. 9B and C, respectively. It can be seen that the binding energy of Ti 2p almost keeps unchanged, while the binding energy of O 1s reduced 0.4 eV (from 529.8 eV to 529.4 eV) after loading of Au-NRs, reflecting the strong interaction between Au-NRs and TiO_2-HNBs. Fig. 9D is the high resolution XPS spectrum of Au 4f for Au-NRs/TiO_2-HNBs photocatalyst, where two peaks with binding energies of 86.5 eV and 82.9 eV are corresponding to Au $4f_{5/2}$ and Au $4f_{7/2}$ orbit energies, respectively (Yuan et al., 2007). The binding energy of bulk metallic gold (Au^0) is usually at about 84.0 eV. However, in Au-NRs/TiO_2-HNBs, the binding energy of Au $4f_{7/2}$ negatively shifts 1.1 eV, which can be interpreted as a result of interaction between Au-NRs and the surface Ti^{3+} centers at defects in TiO_2-HNBs (Golabiewska et al., 2016). The Au^0 $4f_{7/2}$ with binding energy of 82.9 eV has also been observed on gold nanodots modified TiO_2 sample, which has been ascribed to the strong interactions between Au nanodots and TiO_2 nanoparticles (Wang et al., 2009).

Further study shows that the presence of Au-NRs has little effect of the BET surface areas of the photocatalyst (Fig. 10). The BET surface areas for Au-NRs, Au-NPs and Au-NSs loaded TiO_2-HNBs are 51.0, 56.7 and 55.7 $m^2\ g^{-1}$, respectively, similar to that of pristine TiO_2-NHBs (52.0 $m^2\ g^{-1}$) (Huang et al., 2013). Therefore, BET surface area is not the key factor that affects the photoreactivity of TiO_2-HNBs.

3.4. Photocatalytic activity

The photocatalytic activity of the photocatalysts were compared by photocatalytic degradation of RhB dye and NO oxidation. From Fig. 11A, it can be seen that RhB shows little degradation in the absence of photocatalyst even under the irradiation of an Xe lamp. The photocatalytic degradation of RhB accelerates in the presence of TiO_2-HNBs due to the attacks of ROSs such as $^{\bullet}OH$ and $^{\bullet}O_2^-$. After loading with Au nanoparticles, the degradation of RhB is sharply increased, indicating the positive effect of Au nanoparticles on the photocatalytic activity of TiO_2-HNBs. The degradation cuves of RhB can be fitted with pseudo-1st-order kinetics, and the degradation rate constants are shown in Fig. 11B. It can be seen that the photocatalytic activity of TiO_2-HNBs improved 4.2 times, from 0.00444 min^{-1} to 0.0187 min^{-1} after modified by Au-NRs. Au-NRs/TiO_2-HNBs also exhibits excellent photocatalytic stability (Fig. 12). Its photocatalytic activity almost keeps unchanged even recycling use 5 times for RhB degradation, indicating that it is promising to be practical applications.

On considering that RhB can also be degraded through photosensitization pathway (Zhao et al., 2018), the photocatalytic activity of the photocatalyst was also evaluated by NO oxidation, and the results are shown in Fig. 13. It can also be seen the improved photocatalytic of Au nanoparticles modified TiO_2-HNBs, which is consistent with results for RhB degradation (Fig. 11).

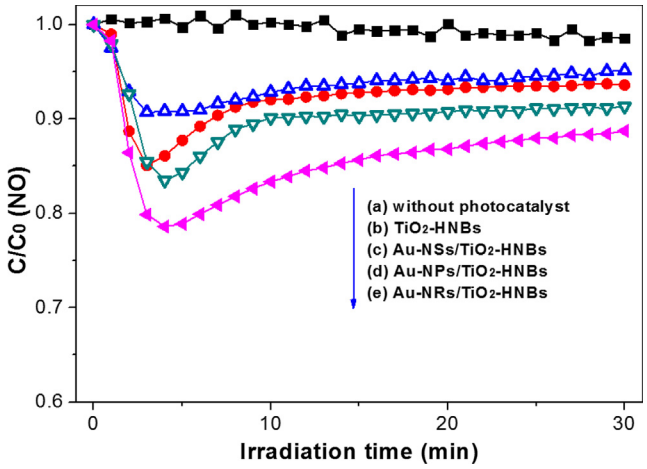

Fig. 13 Visible photocatalytic oxidation curves of NO over different photocatalysts.

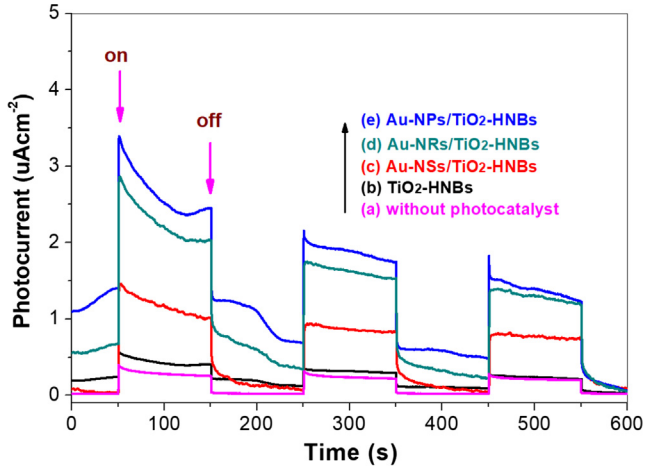

Fig. 14 Transient photocurrents of the prepared photocatalysts under visible LED lamp irradiation ($\lambda > 420$ nm).

3.5. Mechanism

To account for the enhanced visible photoreactivity of TiO_2-HNBs, transient photocurrents were measured for all the photocatalysts (details see part S3 of the Supporting Information), as the value of photocurrent can indirectly reflect the ability of semiconductor photocatalyst to generate and transfer of photo-generated charge carriers under irradiation (Liang et al., 2017; Lv et al., 2012a). From Fig. 14, it can be clearly seen that the visible photocurrent of TiO_2-HNBs sharply increases after modified with Au nanoparticles. The photocurrent of the photocatalyst follows the decreasing order of Au-NRs/TiO_2-HNBs (2.2 uAcm^{-2}) > Au-NPs/TiO_2-HNBs (2.0 uAcm^{-2}) > Au-NSs/TiO_2-HNBs (1.4 uAcm^{-2}) > TiO_2-HNBs (0.3 uAcm^{-2}), which can be ascribed to the strongest SPR effect of Au-NRs among all the gold modified TiO_2 photocatalyst. Note that the photocurrent of pristine TiO_2-HNBs is negligible as it is almost the same as that of the control experiment (without photocatalyst). From Fig. 14, we can also see that all the photocurrents decrease as irradiation time, which may be due to the fact that the TiO_2/ITO film in Na_2SO_4 solution is unstable, as some photocatalyst powders falling down from the film. Then we can understand the non-linear photocurrent during irradiation period.

The bandgap of anatase TiO_2 is about 3.2 eV. Therefore, TiO_2-HNBs can not be excited under visible irradiation. The sharply increased photocurrents of Au/TiO_2-HNBs should come from the SPR effect of Au nanoparticles. As the fermi energy level of Au nanoparticles is higher than conduction band of anatase TiO_2 (Wang et al., 2009); hot electrons can transfer from Au nanoparticles to the conduction band of anatase TiO_2-HNBs, which are then captured by adsorbed O_2 on the surface of TiO_2-HNBs, forming $\cdot O_2^-$, while holes are left on the surface of Au nanoparticles (Golabiewska et al., 2016). Both $\cdot O_2^-$ radicals and holes are ROSs, which are responsible for the degradation of RhB and NO oxidation (Scheme 2).

Note that the loading amounts of Au nanoparticles on the surface of TiO_2-HNBs are the same among three different Au/TiO_2-HNBs photocatalysts. As for Au, the particle morphology plays a more significant role on the properties of the SPR band than size (Yuan et al., 2007). The strongest SPR

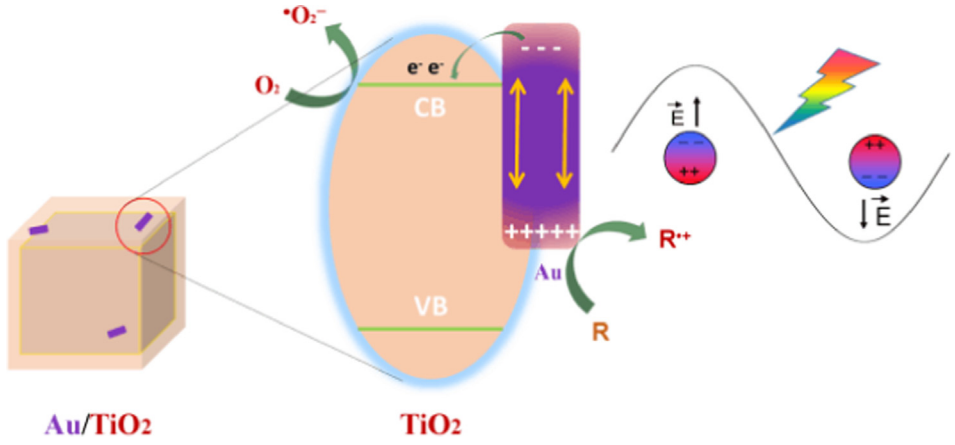

Scheme 2 Proposed mechanism illustrating the SPR effect of Au on enhanced visible photoreactivity of Au/TiO_2-HNBs hybridized photocatalyst.

effect of Au-NRs makes Au-NRs/TiO_2-HNBs exhibits the highest visible photocatalytic activity when compared with Au-NSs/ TiO_2-HNBs and Au-NPs/TiO_2-HNBs.

4. Conclusions

Au nanoparticles sensitized TiO_2-HNBs hybridized photocatalyst was successfully prepared. The shape of the Au nanoparticles has a significant impact on the visible photocatalytic activity of the Au/TiO_2-HNBs. When compared with Au-NSs and Au-NPs, Au-NRs modified TiO_2-HNBs exhibit the highest visible photocatalytic activity towards RhB degradation and NO oxidation. The enhanced visible photocatalytic activity of Au/TiO_2-HNBs is attributed to the SPR effect of Au nanoparticles. The conduction band of TiO_2-HNBs facilitates the capture of hot electrons from the illuminated Au nanoparticles to form $\cdot O_2^-$ radicals, retarding the recombination of charge carrier. Au-NRs/TiO_2-HNBs hybridized photocatalyst shows the highest visible photoreactivity and excellent photocatalytic stability, indicating that it is promising to be practically used in pollution control.

Conflicts of interest

There are no conflicts to declare.

Acknowledgements

This work was supported by National Natural Science Foundation of China (21177161, 31402137 and 51672312) and Science Foundation of Hubei Province for Distinguished Young Scholars (2013CFA034) and the Program for Excellent Talents in Hubei Province (RCJH15001), funded by the Opening Project of Key Laboratory of Green Catalysis of Sichuan Institutes of High Education (LYZ1107) and the Fundamental Research Funds for the Central Universities, South-Central University for Nationalities (CZP17077 and CZP19006).

Appendix A. Supplementary material

Supplementary data to this article can be found online at https://doi.org/10.1016/j.arabjc.2019.08.011.

References

Acik, I.O., Dolgov, L., Krunks, M., Mere, A., Mikli, V., Pikker, S., Loot, A., Sildos, I., 2014. Surface plasmon resonance caused by gold nanoparticles formed on sprayed TiO_2 films. Thin Solid Films 553, 144–147.

Akple, M.S., Low, J.X., Qin, Z.Y., Wageh, S., Al-Ghamdi, A.A., Yu, J.G., Liu, S.W., 2015. Nitrogen-doped TiO_2 microsheets with enhanced visible light photocatalytic activity for CO_2 reduction. Chin. J. Catal. 36, 2127–2134.

Borisyuk, P.V., Troyan, V.I., Pushkin, M.A., Borman, V.D., Tronin, V.N., 2012. Blue and red shifts of interband transition energy in supported Au nanoclusters on SiO_2 and HOPG investigated by reflection electron energy-loss spectroscopy. J. Nanosci. Nanotech. 12, 8751–8754.

Damato, C.A., Giovannetti, R., Zannotti, M., Rommozzi, E., Ferraro, S., Seghetti, C., Minicucci, M., Gunnella, R., Cicco, A.D., 2018. Enhancement of visible-light photoactivity by polypropylene coated plasmonic Au/TiO_2 for dye degradation in water solution. Appl. Surf. Sci. 441, 575–587.

Di, T.M., Zhang, J.F., Cheng, B., Yu, J.G., Xu, J.S., 2018. Hierarchically nanostructured porous TiO_2(B) with superior photocatalytic CO_2 reduction activity. Sci. Chin. Chem. 61, 344–350.

Duan, Y.Y., Liang, L., Lv, K.L., Li, Q., Li, M., 2018. TiO_2 faceted nanocrystals on the nanofibers: homojunction TiO_2 based Zscheme photocatalyst for air purification. Appl. Surf. Sci. 456, 817–826.

Dwivedi, C., Dutta, V., 2012. Size controlled synthesis and photocatalytic activity of anatase TiO_2 hollow microspheres. Appl. Surf. Sci. 258, 9584–9588.

Fujishima, A., Honda, K., 1972. Electrochemical photolysis of water at a semiconductor electrode. Nature 238, 37–38.

Golabiewska, A., Malankowska, A., Jarek, M., Lisowski, W., Nowaczyk, G., Jurga, S., Zaleska-Medynska, A., 2016. The effect of gold shape and size on the properties and visiblelight-induced photoactivity of Au-TiO_2. Appl. Catal. B 196, 27–40.

He, Q.R., Sun, H., Shang, Y.X., Tang, Y.N., She, P., Zeng, S., Xu, K. L., Lu, G.L., Liang, S., Yin, S.Y., Liu, Z.N., 2018. Au@TiO_2 yolk-shell nanostructures for enhanced performance in both photoelectric and photocatalytic solar conversion. Appl. Surf. Sci. 441, 458–465.

Huang, Z.A., Wang, Z.Y., Lv, K.L., Zheng, Y., Deng, K.J., 2013. Transformation of TiOF2 cube to a hollow nanobox assembly from anatase TiO2 nanosheets with exposed 001 facets via solvothermal strategy. ACS Appl. Mater. Interf. 5, 8663–8669.

Huang, Z.A., Sun, Q., Lv, K.L., Zhang, Z.H., Li, M., Li, B., 2015. Effect of contact interface between TiO_2 and g-C_3N_4 on the photoreactivity of g-C_3N_4/TiO_2 photocatalyst: (001) vs (101) facets of TiO_2. Appl. Catal. B 164, 420–427.

Lan, J.F., Wu, X.F., Lv, K.L., Si, L.L., Deng, K.J., 2015. Fabrication of TiO_2 hollow microspheres using $K_3PW_{12}O_{40}$ as template. Chin. J. Catal. 36, 2237–2243.

Lei, C.X., Jiang, X.L., Huang, X., Liu, X., Zeng, D.Q., Ma, Y.T., Wang, L.S., Peng, D.L., 2015. Improved liquid phase deposition of anatase TiO2 hollow microspheres with exposed 001 facets and their photocatalyticactivity. Appl. Surf. Sci. 359, 860–867.

Li, Y.Y., Cao, S.B., Zhang, A., Zhang, C., Qu, T., Zhao, Y.B., Chen, A.H., 2018b. Carbon and nitrogen co-doped bowl-like Au/TiO_2 nanostructures with tunable size for enhanced visible-light-driven photocatalysis. Appl. Surf. Sci. 445, 350–358.

Li, Y.H., Ho, W.K., Lv, K.L., Zhu, B.C., Lee, S.C., 2018c. Carbon vacancy-induced enhancement of the visible light-driven photocatalytic oxidation of NO over g-C_3N_4 nanosheets. Appl. Surf. Sci. 430, 380–389.

Li, X.F., Lv, K.L., Deng, K.J., Tang, J.F., Su, R., Sun, J., Chen, L.Q., 2009. Synthesis and characterization of ZnO and TiO_2 hollow spheres with enhanced photoreactivity. Mater. Sci. Eng. B 158, 40–47.

Li, Y.H., Lv, K.L., Ho, W.K., Zhao, Z.W., Yu, H., 2017b. Enhanced visible-light photo-oxidation of nitric oxide using bismuth-coupled graphitic carbon nitride composite heterostructures. Chin. J. Catal. 38, 321–329.

Li, Y.H., Lv, K.L., Ho, W.K., Dong, F., Wu, X.F., Xia, Y., 2017a. Hybridization of rutile TiO_2 (rTiO_2) with g-C_3N_4 quantum dots (CN QDs): an efficient visible-light-driven Z-scheme hybridized photocatalyst. Appl. Catal. B 202, 611–619.

Li, Y.H., Wu, X.F., Ho, W.K., Lv, K.L., Li, Q., Li, M., Lee, S.C., 2018d. Graphene-induced formation of visible-light-responsive SnO_2-Zn_2SnO_4 Z-scheme photocatalyst with surface vacancy for the enhanced photoreactivity towards NO and acetone oxidation. Chem. Eng. J. 336, 200–210.

Li, X., Xie, J., Jiang, C.J., Yu, J.G., Zhang, P.Y., 2018a. Review on design and evaluation of environmental photocatalysts. Front. Environ. Sci. Eng. 12, 14.

Liang, L., Li, K.N., Lv, K.L., Ho, W.K., Duan, Y.Y., 2017. Highly photoreactive TiO_2 hollow microspheres with super thermal stability for acetone oxidation. Chin. J. Catal. 38, 2085–2093.

Lou, X.W., Archer, L.A., Yang, Z.C., 2008. Hollow micro-/nanostructures: synthesis and applications. Adv. Mater. 20, 3987–4019.

Low, J.X., Cheng, B., Yu, J.G., 2017. Surface modification and enhanced photocatalytic CO_2 reduction performance of TiO_2: a review. Appl. Surf. Sci. 392, 658–686.

Low, J.X., Qiu, S.Q., Xu, D.F., Jiang, C.J., Cheng, B., 2018a. Direct evidence and enhancement of surface plasmon resonance effect on Ag-loaded TiO_2 nanotube arrays for photocatalytic CO_2 reduction. Appl. Surf. Sci. 434, 423–432.

Low, J.X., Zhang, L.Y., Zhu, B.C., Liu, Z.Y., Yu, J.G., 2018b. TiO_2 photonic crystals with localized surface photothermal effect and enhanced photocatalytic CO_2 reduction activity. ACS Sust. Chem. Eng. 6, 15653–15661.

Low, J.X., Zhang, L.Y., Tong, T., Shen, B.J., Yu, J.G., 2018c. TiO_2/MXene Ti_3C_2 composite with excellent photocatalytic CO_2 reduction activity. J. Catal. 361, 255–266.

Luan, Y.B., Jing, L.Q., Xie, Y., Sun, X.J., Feng, Y.J., Fu, H.G., 2013. Exceptional photocatalytic activity of 001-facet-exposed TiO_2 mainly depending on enhanced adsorbed oxygen by residual hydrogen fluoride. ACS Catal. 3, 1378–1385.

Lv, K.L., Hu, J.C., Li, X.H., Li, M., 2012a. Cysteine modified anatase TiO_2 hollow microspheres with enhanced visible-light-driven photocatalytic activity. J. Mol. Catal. A 356, 78–84.

Lv, K.L., Cheng, B., Yu, J.G., Liu, G., 2012b. Fluorine ions-mediated morphology control of anatase TiO_2 with enhanced photocatalytic activity. Phys. Chem. Chem. Phys. 14, 5349–5362.

Lv, K.L., Fang, S., Si, L.L., Xia, Y., Ho, W.K., Li, M., 2017. Fabrication of TiO_2 nanorod assembly grafted rGO (rGO@TiO2-NR) hybridized flake-like photocatalyst. Appl. Surf. Sci. 391, 218–227.

Ma, Y.T., Li, Z.H., 2018. Coupling plasmonic noble metal with TiO_2 for efficient photocatalytic transfer hydrogenation: M/TiO_2 (M = Au and Pt) for chemoselective transformation of cinnamaldehyde to cinnamyl alcohol under visible and 365 nm UV light. Appl. Surf. Sci. 452, 279–285.

Meng, A.Y., Zhu, B.C., Zhong, B., Zhang, L.Y., Cheng, B., 2017. Direct Z-scheme TiO_2/CdS hierarchical photocatalyst for enhanced photocatalytic H_2-production activity. Appl. Surf. Sci. 422, 518–527.

Negrín-Montecelo, Y., Comesaña-Hermo, M., Kong, X.T., Rodríguez-González, B., Wang, Z.M., Pérez-Lorenzo, M., Govorov, A. O., Correa-Duarte, M.A., 2018. Traveling hot spots in plasmonic photocatalysis: manipulating interparticle spacing for real-time control of electron injection. ChemCatChem 10, 1561–1565.

Ning, X., Wei, F.X., Fu, H.Y., Qu, X.L., Xu, Z.Y., Zheng, S.R., 2018. Enhanced catalytic reduction of 4-nitrophenol over titania nanotube supported gold nanoparticles by weak ultraviolet light irradiation: role of gold surface charge. Appl. Surf. Sci. 445, 535–541.

Panayotov, D.A., Burrows, S.P., Yates, J.T., Morris, J.R., 2011. Mechanistic studies of hydrogen dissociation and spillover on Au/TiO_2: IR spectroscopy of coadsorbed CO and H-donated electrons. J. Phys. Chem. C 115, 22400–22408.

Priebe, J.B., Radnik, J., Kreyenschulte, C., Lennox, A.J.J., Junge, H., Beller, M., Brückner, A., 2017. H_2 generation with (mixed) plasmonic Cu/Au-TiO_2 photocatalysts: structure-reactivity relationships assessed by in situ spectroscopy. ChemCatChem 9, 1025–1031.

Qi, K.Z., Cheng, B., Yu, J.G., Ho, W.K., 2017. A review on TiO_2-based Z-scheme photocatalysts. Chin. J. Catal. 38, 1936–1955.

Rahul, T.K., Sandhyarani, N., 2017. In situ gold-loaded fluorinated titania inverse opal photocatalysts for enhanced solar-light-driven hydrogen production. ChemNanoChem 3, 503–510.

Schneider, J., Matsuoka, M., Takeuchi, M., Zhang, J.L., Horiuchi, Y., Anpo, M., Bahnemann, D.W., 2014. Understanding TiO_2 photocatalysis: mechanisms and materials. Chem. Rev. 114, 9919–9986.

Sheng, J.Y., Li, X.J., Xu, Y.M., 2014. Generation of H_2O_2 and OH radicals on Bi_2WO_6 for phenol degradation under visible light. ACS Catal. 4, 732–737.

Shi, T., Duan, Y.Y., Lv, K.L., Hu, Z., Li, Q., Li, M., Li, X.F., 2018. Photocatalytic oxidation of acetone over high thermally stable TiO_2 nanosheets with exposed (001) facets. Front. Chem. 6, 175.

Verbruggen, S.W., Keulemans, M., Filippousi, M., Flahaut, D., Tendeloo, G.V., Lacombe, S., Martens, J.A., Lenaerts, S., 2014. Plasmonic gold–silver alloy on TiO_2 photocatalysts with tunable visible light activity. Appl. Catal. B 156–157, 116–121.

Wanbayor, R., Ruangpornvisuti, V., 2012. A periodic DFT study on binding of Pd, Pt and Au on the anatase TiO_2 (001) surface and adsorption of CO on the TiO_2 surface-supported Pd, Pt and Au. Appl. Surf. Sci. 258, 3298–3301.

Wang, W., Lai, M., Fang, J.J., Lu, C.H., 2018. Au and Pt selectively deposited on {001}-faceted TiO_2 toward SPR enhanced photocatalytic Cr(VI) reduction: the influence of excitation wavelength. Appl. Surf. Sci. 439, 430–438.

Wang, Z.Y., Lv, K.L., Wang, G.H., Deng, K.J., Tang, D.G., 2010. Study on the shape control and photocatalytic activity of high-energy anatase titania. Appl. Catal. B 100, 378–385.

Wang, P., Xie, T.F., Li, H.Y., Peng, L., Zhang, Y., Wu, T.S., Pang, S., Zhao, Y.F., Wang, D.J., 2009. Synthesis and plasmon-induced charge-transfer properties of monodisperse gold-doped titania microspheres. Chem. Eur. J. 15, 4366–4372.

Wang, Y., Yu, J.G., Xiao, W., Li, Q., 2014. Microwave-assisted hydrothermal synthesis of graphene based Au-TiO_2 photocatalysts for efficient visible-light hydrogen production. J. Mater. Chem. A 2, 3847–3855.

Wu, X., Song, H., Yoon, J., Yu, Y., Chen, Y., 2009. Synthesis of core-shell Au@TiO_2 nanoparticles with truncated wedge-shaped morphology and their photocatalytic properties. Langmuir 25, 6438–6447.

Yang, R.W., Cai, J.H., Lv, K.L., Wu, X.F., Wang, W.G., Xu, Z.H., Li, M., Li, Q., Xu, W.Q., 2017a. Fabrication of TiO_2 hollow microspheres assembly from nanosheets (TiO_2-HMSs-NSs) with enhanced photoelectric conversion efficiency in DSSCs and photocatalytic activity. Appl. Catal. B 210, 184–193.

Yang, J.J., Liu, B.S., Zhao, X.J., 2017b. A visible-light-active Au-Cu(I)@$Na_2Ti_6O_{13}$ nanostructured hybrid pasmonic photocatalytic membrane for acetaldehyde elimination. Chin. J. Catal. 38, 2048–2055.

Yang, Z.L., Lu, J., Ye, W.C., Yu, C.S., Chang, Y.L., 2017c. Preparation of Pt/TiO_2 hollow nanofibers with highly visible light photocatalytic activity. Appl. Surf. Sci. 392, 472–480.

Yang, H.G., Sun, C.H., Qiao, S.Z., Zou, J., Liu, G., Smith, S.C., Cheng, H.M., Lu, G.Q., 2008. Anatase TiO_2 single crystals with a large percentage of reactive facets. Nature 453, 638–641.

Yu, K.F., Tianw, Y., Tatsuma, T., 2006. Size effects of gold nanaoparticles on plasmon-induced photocurrents of gold-TiO_2 nanocomposites. Phys. Chem. Chem. Phys. 8, 5417–5420.

Yuan, H., Ma, W.H., Chen, C.C., Zhao, J.C., Liu, J.W., Zhu, H.Y., Gao, X.P., 2007. Shape and SPR evolution of thorny gold nanoparticles promoted by silver ions. Chem. Mater. 19, 1592–1600.

Zhang, D.N., Ma, X.Y., Zhang, H.W., Liao, Y.L., Xiang, Q.J., 2018a. Enhanced photocatalytic hydrogen evolution activity of carbon and nitrogen self-doped TiO_2 hollow sphere with the creation of oxygen vacancy and Ti^{3+}. Mater. Today Energy 10, 132–140.

Zhang, G.W., Miao, H., Hu, X.Y., Mu, J.L., Liu, X.X., Han, T.X., Fan, J., Liu, E.Z., Yin, Y.C., Wan, J., 2017. A facile strategy to fabricate Au/TiO_2 nanotubes photoelectrode with excellent photoelectrocatalytic properties. Appl. Surf. Sci. 391, 345–352.

Zhang, C.J., Tian, L.J., Chen, L.Q., Li, X.F., Lv, K.L., Deng, K.J., 2018b. One-pot topotactic synthesis of Ti^{3+} self-doped 3D TiO_2 hollow nanoboxes with enhanced visible light response. Chin. J. Catal. 39, 1373–1383.

Zhang, L., Yang, C., Lv, K.L., Lu, Y.C., Li, Q., Wu, X.F., Li, Y.H., Li, X.F., Fan, J.J., Li, M., 2019. SPR effect of bismuth enhanced visible photoreactivity of Bi_2WO_6 for NO abatement. Chin. J. Catal. 40, 755–764.

Zhao, X., Du, Y.T., Zhang, C.J., Tian, L.J., Li, X.F., Deng, K.J., Chen, L.Q., Duan, Y.Y., Lv, K.L., 2018. Enhanced visible photocatalytic activity of TiO_2 hollow boxes modified by methionine for RhB degradation and NO oxidation. Chin. J. Catal. 39, 736–746.

Zou, Y.J., Shi, J.W., Ma, D.D., Fan, Z.Y., Niu, C.M., Wang, L.Z., 2017. Fabrication of g-C_3N_4/Au/C-TiO_2 hollow structures as visible-light-driven Z-scheme photocatalysts with enhanced photocatalytic H_2 evolution. ChemCatChem 9, 3752–3761.